MODELING A TWO-LINK RIGID SWIMMER SCALLOPING IN LINEAR VISCOELASTIC FLUID

by

Tania Ullah

SUBMITTED TO THE DEPARTMENT OF MECHANICAL ENGINEERING IN PARTIAL FULFILLMENT OF THE REQUIREMENTS FOR THE DEGREE OF

BACHELOR OF SCIENCE
AT THE
MASSACHUSETTS INSTITUTE OF TECHNOLOGY

JUNE 2007

Signature of Author: .....
Department of Mechanical Engineering
May 11, 2007

Certified by: .....
Anette Hosoi
Associate Professor of Mechanical Engineering
Thesis Supervisor

Accepted by: .....
John H. Lienhard, V
Professor of Mechanical Engineering
Chairman, Undergraduate Thesis Committee

[Page Intentionally Left Blank]

Modeling a Two-Link Rigid Swimmer Scalloping in Linear Viscoelastic Fluid

by

Tania Ullah

Submitted to the Department of Mechanical Engineering on May 11, 2007
in partial fulfillment of the requirements for the Degree of
Bachelor of Science in Mechanical Engineering.

Abstract

In his renowned lecture on *Life at low Reynolds number*, E.M. Purcell established that a rigid swimmer comprised of two links cannot swim in a viscous Newtonian fluid due to the reciprocal nature of its movements. Viscoelastic fluid, on the other hand, has a characteristic time scale associated with stress relaxation and can impart asymmetrical stresses on the body of a swimmer to propel it forward. This work focuses on developing a theoretical model for the fluid-structure interactions that influence the swimming of a two-link specimen in viscoelastic fluid. Because the oscillation of the slender rods that comprise the links of the swimmer elicit a response from the surrounding fluid at various frequencies, the modeling consisted of a complex Fourier analysis. This paper discusses in detail the physics of the specimen's swimming and the equations that govern its movement in the fluid. The work done has been purely theoretical; however, a numerical simulation to validate the theory will be conducted as future work.

Thesis Supervisor: Anette Hosoi
Title: Associate Professor, Department of Mechanical Engineering

Acknowledgements

I would first like to thank my thesis advisor, Professor Anette Hosoi, who has guided me on this and other related projects for the past year and a half. I came to her as an eager UROP student and she has helped me develop my interest in fluid and solid mechanics. Professor Hosoi has worked closely with me to produce the work that is in this paper and I could not have accomplished what I did without her help.

A special thanks is extended to all the female faculty in the Mechanical Engineering Department who have been exceptional role models to women students at MIT. Their work, encouragement and advice have inspired me to pursue my graduate studies in Mechanical Engineering. I hope to follow in their footsteps.

Last, but certainly not least, I would like to thank my parents who wanted their children to have the education they never received. Their love and support throughout the years has made obtaining my degree possible. This thesis is dedicated to them.

Table of Contents

List of Figures

Chapter 1

Introduction

The objective of this thesis is to develop a model of a two-link rigid swimmer in viscoelastic fluid. A brief background on locomotion at low Reynolds numbers and the material characteristics of viscoelastic fluids are presented in this chapter. In Chapter 2, a preliminary model is developed in order to understand the physics of the two-link swimmer scalloping in a Newtonian fluid. Finally, Chapter 3 discusses the theoretical approach taken to model the swimmer in viscoelastic fluid.

1.1 Background

1.1.1 E.M. Purcell's *Life at low Reynolds number*

Marine propulsion has long been a topic of interest for mechanical and ocean engineers. The intuition naval engineers have developed in order to design efficient ships, submarines, and other watercraft, however, applies only to large-scale fluid-structure interactions. The mechanics and dynamics of fluid flow on the scale of tens of yards are generally in the high Reynolds number regime. Recall that the Reynolds number is a dimensionless ratio of the inertial and viscous forces. Consequently, when the Reynolds number is large the inertia of the fluid dominates its flow characteristics.

If one is not interested in the fluid mechanics associated with propeller motion in the turbulent ocean, but interested in the locomotion of microorganisms or tiny swimmers in viscous fluids, we must enter the world of low Reynolds number fluid phenomena. In this regime, inertia becomes irrelevant. As E.M. Purcell stated in his renowned lecture *Life at low Reynolds number*, the square of a fluid's viscosity divided by its density gives a measure of the force required to tow an object in that fluid [1]. Hence, relatively large propulsive forces are required to move about in highly viscous fluids and bodies

experience relatively large drag forces. The velocities associated with their movements are small. Thus, the effects of inertia are insignificant at low Reynolds numbers.

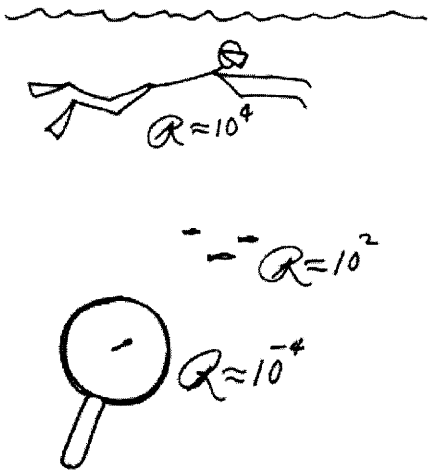

Figure 1-1: Slide from E.M. Purcell's renowned lecture depicting various swimmers and indicating their Reynolds numbers (figure reproduced from [1]). The first is a man, the second is a group of fish and the third is a microorganism.

The time scale associated with low Reynolds number locomotion is large and rates of change are small. In his lecture, Purcell asks the audience to consider a man swimming at the same Reynolds number as his own sperm [1]. He would be immersed in a pool of molasses and would move only a few meters every couple of weeks. In this case, time also makes no difference and the only factor in propulsion is the deformation, or configuration, of the swimming body. The insignificance of inertia, and by extension time, make low Reynolds number fluid phenomena distinct from those at high Reynolds number.

1.1.2 Reciprocal Motion and the Scallop Theorem

As established earlier, time parameterization plays no role in the fluid-structure interaction for low Reynolds number locomotion; a swimmer can deform its body in the same manner quickly or slowly, its motion will be no different [1]. Therefore, the propulsive forces imparted on the swimmer by the surrounding Newtonian fluid depend

only on the swimmer's configuration. As such, Purcell contends that reciprocal motion in a Newtonian fluid results in no net motion [1]. By reciprocal motion he means a series of shape changes that a swimming body undergoes such that the forward sequence is identical to the sequence played in reverse. Any progress that a swimmer makes will be undone in the reverse sequence.

"The Scallop Theorem," as stated by Purcell, says that a scallop in Newtonian fluid at low Reynolds numbers will experience no net displacement no matter the pattern of its movements. A scallop normally moves through a fluid by opening its shell and closing it quickly. At low Reynolds numbers the scallop will not move because it has one hinge and only one degree of freedom in its configuration [1]; it is bound to make reciprocal motions. A swimmer that has three links, and therefore two hinges, can manage to swim with non-reciprocal motions (see Fig. 1-2). As for the swimmer that has N links and N-1 degrees of freedom, there are a great many configurations that the swimmer can undergo and that will result in non-reciprocal motion as well. Such swimmers, with links N>2, escape the symmetry that traps a two-link swimmer in one place.

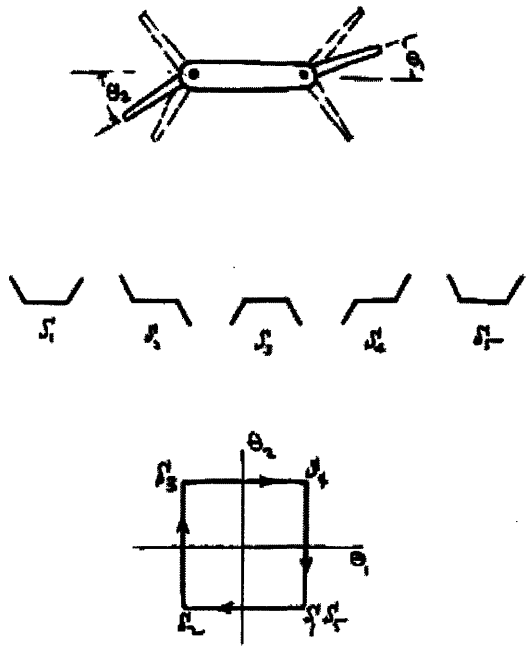

Figure 1-2: A three-link swimmer whose motions are non-reciprocal (reproduced from [1]).

1.1.3 Viscoelastic fluids

At this point, it has been established how a two-link swimmer behaves in Newtonian fluid at low Reynolds numbers. The symmetry present in the reciprocal motions of the scallop prevents it from swimming anywhere. The goal of this thesis is to determine a model for this swimmer when it is attempting to move about in viscoelastic fluid. Viscoelastic fluids are also called "memory fluids" because the past history of deformation contributes to its present stress state [2]. This influence of time on the stress and strain states of the fluid, and therefore on the rigid swimmer it interacts with, will provide the asymmetry needed to propel the swimmer. The two-link rigid swimmer can indeed defy the Scallop Theorem in viscoelastic fluid.

It is appropriate now to provide a comparison between the behaviors of Newtonian and non-Newtonian (specifically viscoelastic) fluids. The shear stress in a Newtonian fluid is linearly proportional to the shear strain rate by a constant of proportionality, called the viscosity. Eq. 1.1 is called *Newton's law of viscosity*:

$$\tau = \eta_0 \dot{\gamma} \tag{1.1}$$

where τ is the shear stress, $\dot{\gamma}$ is the time derivative of the shear strain, and η_0 is the viscosity. Furthermore, the viscosity, η_0, is a fluid property and is independent of the strain or strain rate. Common fluids such as air and water are Newtonian. Some non-Newtonian fluids are ketchup and toothpaste. Ketchup experiences "shear thinning," which means that at higher strain rates the viscosity decreases. Toothpaste is termed "plastic" because it does not begin to deform, or flow, until a finite stress level has been reached [3].

A viscoelastic fluid, as the name indicates, possesses qualities of both viscous and elastic materials. In fact, viscoelastic material properties and functions are generally applicable to both fluids and solids, and the distinction between a viscoelastic fluid and a viscoelastic solid is somewhat blurred [2]. Granite and glacial ice, for example, will experience creep and flow under its own weight. Even water can rupture as a solid when subjected to a large enough stress applied rapidly [2].

Fig. 1-3 shows the comparative response of Newtonian (linear viscous), Hookean (elastic) and viscoelastic materials undergoing constant shear stress (I), constant shear strain and strain rate (II), and an oscillatory shear strain (III).

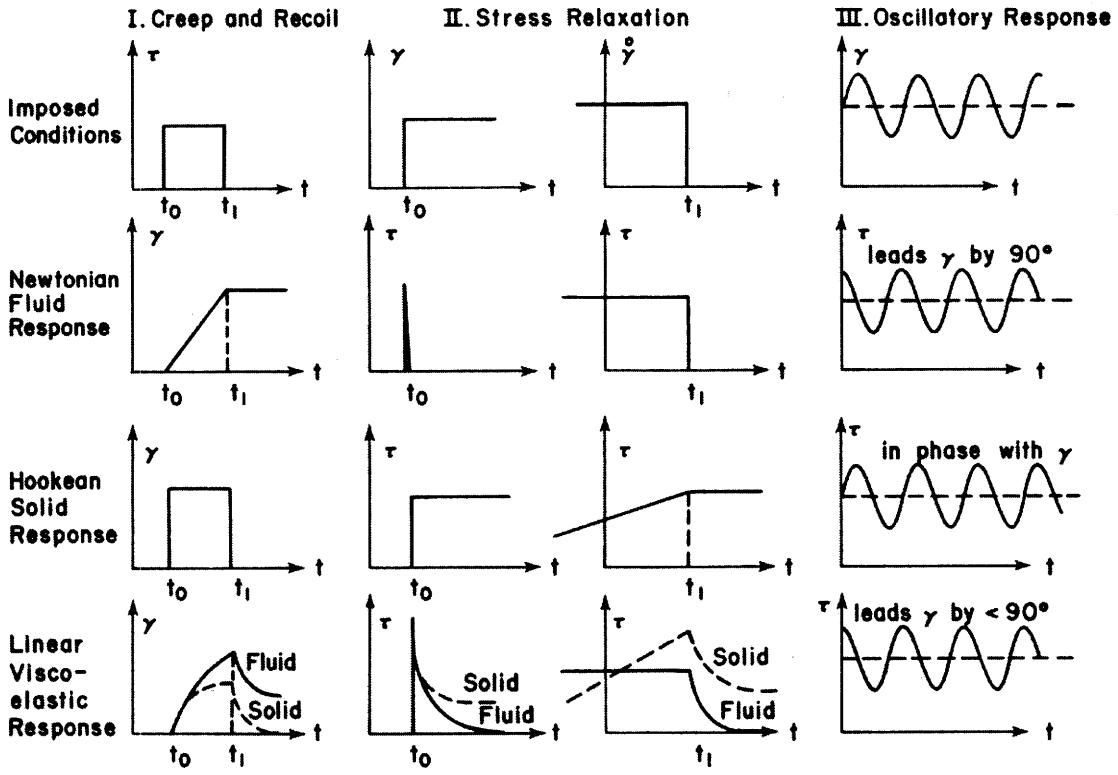

Figure 1-3: Comparative response of Newtonian (viscous), Hookean (elastic) and viscoelastic materials to creep and stress relaxation tests (reproduced from [2]).

For the creep test (I), the viscoelastic material response to a constant shear stress is a non-linear strain increase. After the stress is removed, as it is at $t = t_1$, the material experiences "recoil" and recovers its strain. The Hookean, or elastic, solid response is also to rebound or recover strain but it does so instantaneously. Strain recovery in a viscoelastic material occurs at a finite rate.

As for the stress relaxation test (II), the viscoelastic response to a constant shear strain is to experience an infinite and instantaneous stress. It behaves similarly to the Newtonian, or viscous, fluid in that respect. However, the stress "relaxes" at a finite rate. For a viscoelastic fluid, the stress relaxes to zero.

When a sinusoidal strain is applied to any of the three materials (III), the response is oscillatory in all cases. The Hookean solid experiences no time lag and its stress response is in phase with the strain. The Newtonian fluid response is 90° out of phase with the applied strain. For the viscoelastic fluid, the stress is out of phase by less than 90°, thereby producing both "in-phase" and "out-of-phase" stress response components. The in-phase component of the stress response is due to the elastic and recoverable nature of the fluid deformation. The out-of-phase component is due to its viscous and dissipative nature. An understanding of the oscillatory response of a viscoelastic fluid is particularly important in this work because the movements of the two-link swimmer, and therefore the strain on the surrounding fluid, are oscillatory. The behavior exhibited by the fluid in Fig. 1-3 shows the dual elastic and viscous nature of viscoelastic fluid.

1.1.4 Material Model

The behavior described in the previous section is a result of the combined viscous and elastic nature of viscoelastic fluid. Material models, incorporating analogous mechanical elements, have been developed in order to predict the response of such a fluid for all time and all stress or strain states. The analogous mechanical elements are a dashpot, representing the viscous character, and a spring, representing the elastic character.

One of the simplest constitutive models, the Maxwell model, puts one spring and one dashpot in series. This is the model that has been adopted to characterize the viscoelastic fluid in which the two-link swimmer will move about. Although more accurate constitutive models exist, they are more complex than we need at this stage of our scallop modeling. These include the Voigt and the Standard Linear Solid (SLS) models and they will not be discussed in this paper.

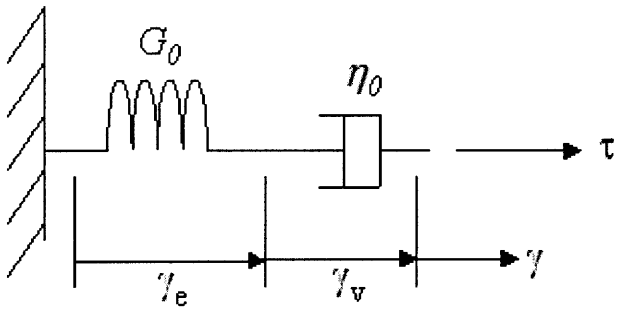

Figure 1-4: Schematic of the Maxwell Model. G_0 is the shear modulus, represented by the spring. η_0 is the viscosity, represented by the dashpot.

Fig. 1-4 illustrates the analogous mechanical model for the Maxwell fluid. A shear stress, τ, is applied to the system. Because the elements are in series, the stress is the same everywhere:

$$\tau_e = \tau_v = \tau \tag{1.2}$$

where the subscript 'e' pertains to the elastic, spring element and the subscript 'v' pertains to the viscous, dashpot element. The shear strain in the spring is:

$$\gamma_e = \frac{\tau}{G_0} \tag{1.3}$$

and the shear strain rate in the dashpot is:

$$\dot{\gamma}_v = \frac{\tau}{\eta_0} \tag{1.4}$$

If the total shear rate is the sum of the shear rates of each element, then the differential equation relating shear stress and strain is:

$$\tau + \lambda\dot{\tau} = \eta_0\dot{\gamma} \tag{1.5}$$

where λ is the characteristic time constant [2]. It is equivalent to:

$$\lambda = \frac{\eta_0}{G_0} \tag{1.6}$$

In order to determine the relaxation modulus for the Maxwell fluid, we subject our model to a constant shear strain, $\gamma = \gamma_0 u(t)$, at $t=0$. $u(t)$ is the unit Heaviside step function. Integrating Eq. 1.5 and recognizing that the initial shear stress is $G_0\gamma_0$ gives us the relaxation modulus.

$$G_R(t) = G_0 e^{-\frac{t}{\lambda}} \tag{1.7}$$

From the relaxation modulus, the stress in the Maxwell fluid can be determined for all strain states and for all time. The expression in Eq. 1.7 will be used later on in this paper when we begin to model the two-link swimmer in a viscoelastic fluid.

1.2 Motivation

Interesting fluids problems with biological relevance have been explored since the 1970s. Studies of flagellar bend propagation, sperm penetration of the egg and sperm motility, however, have mostly involved Newtonian fluids. The motivation of this work is to model swimming behavior that has true applications to biological phenomena.

New Scientist magazine has recently reported on a slew of medical devices that are being developed to aid in the treatment of cardiovascular disease. Chinese engineers have designed a microscopic swimming robot that will deliver drugs to or clear out blockage in the arteries of humans [4]. This tiny robot, measuring 3mm x 2mm x 0.4mm, can maneuver itself along the blood vessels. Miniature sensors [5] and catheters with actuating mechanisms [6] are also being designed to migrate into the blood stream. Concurrently, engineers are working towards shrinking these devices to the scale of a tenth of a millimeter. Locomotion in blood (a non-Newtonian fluid) and on such a small scale provides for unique fluid-structure interactions that we are interested in studying.

New types of biomimetic robots and machines are being developed everyday. Engineers cannot efficiently design them or prescribe their locomotion without having an

understanding of low-Reynolds locomotion in non-Newtonian fluids. In this regard, Professor Hosoi's group in the Hatsopoulos Microfluids Lab has undertaken many projects that have new applications to bioengineering. Studying locomotion in non-Newtonian fluids is giving us insights into the mechanisms with which organisms move about in biofluids. Nature has optimized the swimming of *Helicobacter pylori*, a bacterium responsible for peptic ulcers, within the mucous lining of the stomach's walls. Nature has also optimized the wave motion of snails moving on a thin layer of mucous. Studying swimming mechanisms in non-Newtonian fluids and understanding the optimization animals have mastered in their locomotion is an exciting challenge for mechanical and biological engineers alike.

Chapter 2

Preliminary Model: Newtonian Case

Prior to developing a model for a two-link swimmer in viscoelastic fluid, it was necessary to model the case in which a swimmer is scalloping in a Newtonian fluid. As mentioned earlier, E.M. Purcell and others have established that reciprocal motion, as exhibited by a scallop slowly opening and closing its shell, produces no net motion in a Newtonian fluid at low Reynolds numbers [1]. This chapter discusses the development of a preliminary model—one in which the scalloping swimmer is in Newtonian fluid. In so doing, we 1) verify that, indeed, it has not net motion and 2) gain an understanding of the equations governing the motion of the linked rigid bodies.

2.1 The Swimmer

The figure below (Fig. 2-1) provides a comparison between the swimmer and the scallop after which it was modeled. The swimmer is comprised of two, slender circular rods that are joined and pivot about point O.

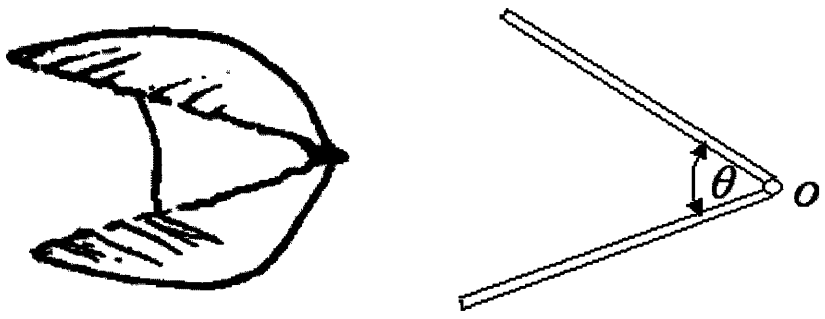

(a) (b)

Figure 2-1: (a) sketch of a scallop (reproduced from [1]) and (b) sketch of the two-link swimmer, whose locomotion is similar to that of a scallop.

Scallops are bivalve mollusks and, as such, have a central adductor muscle that opens and closes their two-part shells [2]. This opening and closing, hereafter referred to as "scalloping," propels the mollusks at relatively high speeds in aquatic environments. Real scallops swim at high Reynolds numbers; the two-link swimmer in this model is the low Reynolds number counterpart. The two-link swimmer undergoes planar motion that mimics the scalloping of a mollusk; the angle between the slender rods, θ, oscillates between a small positive value and a larger positive value (see Fig. 2-2). In the model that is developed, the time-varying angle $\theta(t)$ is prescribed and the observable result is the swimmer's displacement over time.

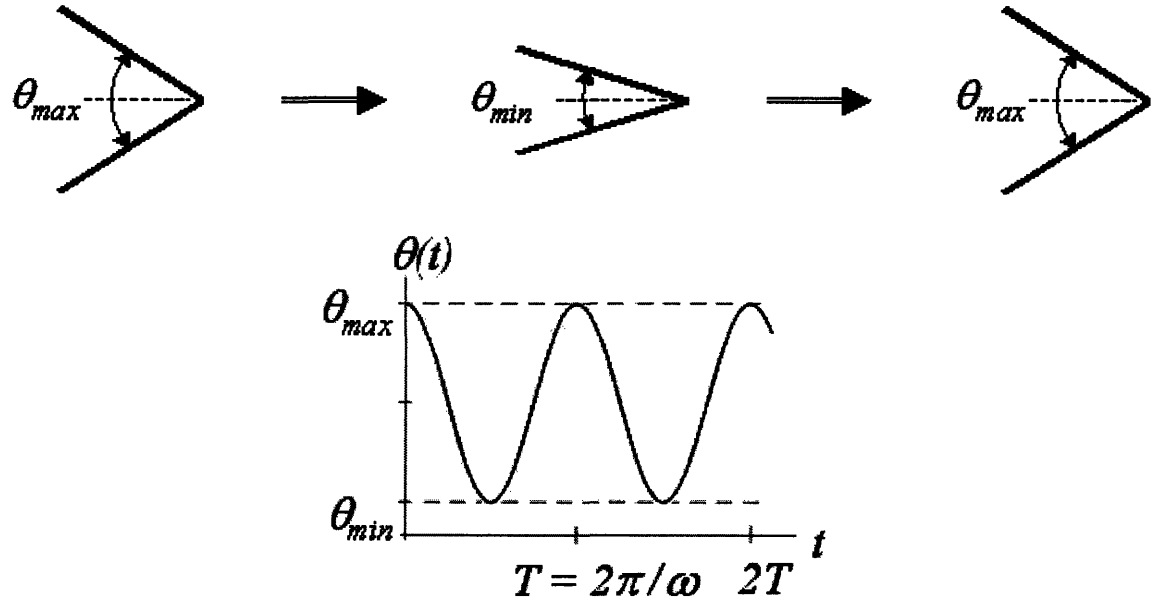

Figure 2-2: Time-varying $\theta(t)$ as the swimmer attempts to propel itself forward.

2.2 Drag Forces

The equations of motion for the scalloping swimmer have been determined using force equilibrium equations, a moment balance equation, velocity boundary conditions and the function forcing $\theta(t)$, the angle between the two arms of the swimmer. To begin the analysis, let us first look at the motion of just one slender rod settling in a viscous, Newtonian fluid. Fig. 2-3 depicts the forces acting on the rod's center of mass, *CM*.

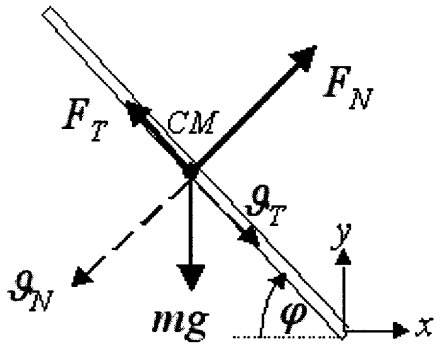

Figure 2-3: A rod settling in a Newtonian fluid at an angle φ, with associated drag forces and weight acting on the rod's center of mass, *CM*. ϑ_T and ϑ_N are the tangential and normal components of the velocity of the rod.

Along with the weight, mg, acting downward, there are tangential and normal drag forces on the long, slender body (F_T and F_N, respectively) in the orientation shown in Fig. 2-3. These retarding forces are components of the viscous drag and are proportional to the center of mass velocity as follows:

$$\begin{aligned} F_T &= C_T \vartheta_T L \\ F_N &= C_N \vartheta_N L \end{aligned} \tag{2.1}$$

where C_T and C_N are the tangential and normal drag coefficients, ϑ_T and ϑ_N are the tangential and normal components of the velocity of the rod, and L is its length. A rod settling in viscous fluid experiences more drag along its length, in the normal direction, than it does in the tangential direction. The coefficients of drag on a slender cylinder in viscous fluid are approximately [3]:

$$\begin{aligned} C_T &= 2\pi\eta_0 \\ C_N &= 4\pi\eta_0 \end{aligned} \tag{2.2}$$

where η_0 is the viscosity of the Newtonian fluid.

In the case of two linked rigid rods, there are two sets of drag forces and two sets of velocity components that interact with each other. Fig. 2-4 is a free body diagram of the two-link swimmer in viscous fluid.

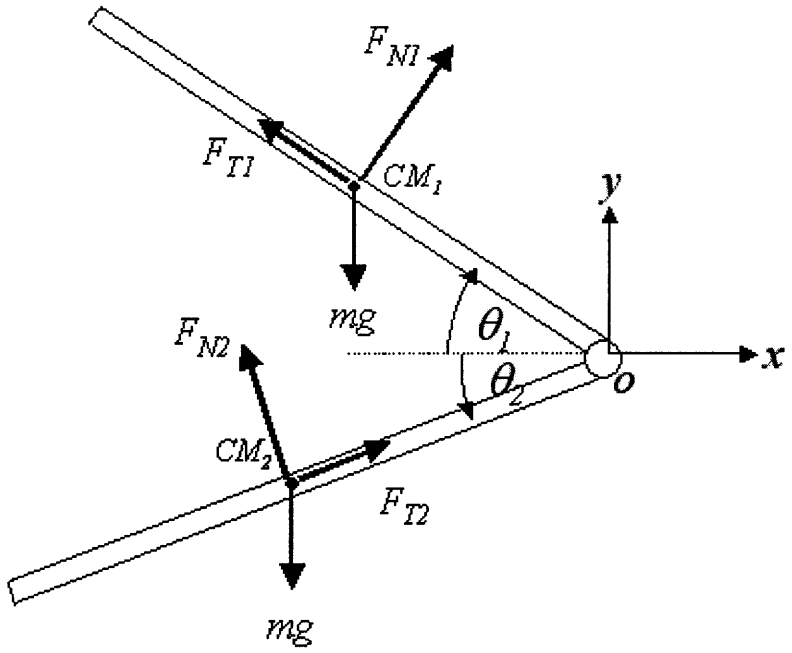

Figure 2-4: Two-link swimmer and its free body diagram. The two arms of the swimmer are joined at point *O*.

The subscript '1' pertains to the drag forces, angle and center of mass of the top rod and the subscript '2' pertains to the drag forces, angle and center of mass of the bottom rod. θ_1 and θ_2 are the positive angles the rods make with the horizontal x-axis.

As the angles change with time, so do the velocities and, therefore, drag forces on the two centers of mass. The time varying quantities associated with the movement of the two-link swimmer are the following variables: $x_1(t)$ and $y_1(t)$, the vertical and horizontal position of the top rod's center of mass; $\theta_1(t)$; $x_2(t)$ and $y_2(t)$, the position of the bottom rod's center of mass; and $\theta_2(t)$. Determining these six unknowns requires six independent equations and they are as follows:

(1) the force equilibrium equation in the x-direction

(2) the force equilibrium equation in the y-direction

(3) the moment equilibrium about point *O*

(4) matching the x-component velocities of the two rods at point *O*

(5) matching the y-component velocities of the two rods at point *O*

(6) a forcing function prescribing the angle between the links as a function of time

The moment equilibrium is taken about point O for convenience. Matching the velocities at point O is a boundary condition that ensures that the ends of the rods are always joined. The forcing of the angles θ_1 and θ_2 will control the scalloping motion of the swimmer and initiate propulsion.

2.3 Equations of Motion

The first two equations relating the unknown variables are the force equilibrium equations:

$$\sum F_x = F_{N1}\sin\theta_1 - F_{T1}\cos\theta_1 - F_{N2}\sin\theta_2 + F_{T2}\cos\theta_2 = 0 \tag{2.3}$$

$$\sum F_y = F_{N1}\cos\theta_1 + F_{T1}\sin\theta_1 + F_{N2}\cos\theta_2 + F_{T2}\sin\theta_2 = 2mg \tag{2.4}$$

The two rods that comprise the swimmer are of equal length L and equal mass m. Eqs. 2.3 and 2.4 are the force balances in the x- and y-directions, respectively. Given that the normal and tangential forces are dependent on the normal and tangential velocity components (see Eq. 2.1), and that the coefficients of drag are known and given by Eq. 2.2, the force balance equations are reduced to:

$$4\pi\eta_0 L\vartheta_{N1}\sin\theta_1 - 2\pi\eta_0 L\vartheta_{T1}\cos\theta_1 - 4\pi\eta_0 L\vartheta_{N2}\sin\theta_2 + 2\pi\eta_0 L\vartheta_{T2}\cos\theta_2 = 0 \tag{2.5}$$

$$4\pi\eta_0 L\vartheta_{N1}\cos\theta_1 + 2\pi\eta_0 L\vartheta_{T1}\sin\theta_1 + 4\pi\eta_0 L\vartheta_{N2}\cos\theta_2 + 2\pi\eta_0 L\vartheta_{T2}\sin\theta_2 = 2mg \tag{2.6}$$

The equations above provide a relation between the tangential and normal components of the velocity and the angles. The variables to be determined, however, are each rod's center of mass x- and y-coordinates. A transformation of coordinates is necessary. Fig. 2-5 is a representation of the velocity vectors.

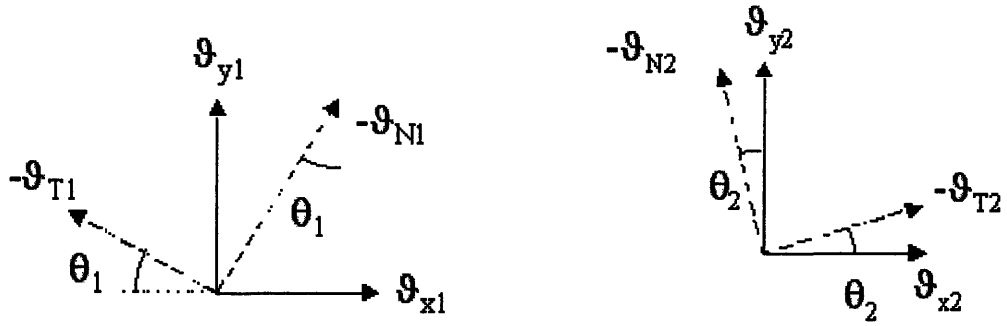

(a) (b)

Figure 2-5: The normal and tangential velocities and equivalent horizontal and vertical velocity components of (a) rod 1 and (b) rod 2.

According to this vector representation, the scalar normal and tangential velocity components can be expressed in terms of the Cartesian velocities by Eq. 2.7 and Eq. 2.8.

$$\begin{aligned} \vartheta_{N1} &= -\vartheta_{x1}\sin\theta_1 - \vartheta_{y1}\cos\theta_1 \\ \vartheta_{T1} &= \vartheta_{x1}\cos\theta_1 - \vartheta_{y1}\sin\theta_1 \end{aligned} \tag{2.7}$$

$$\begin{aligned} \vartheta_{N2} &= \vartheta_{x2}\sin\theta_2 - \vartheta_{y2}\cos\theta_2 \\ \vartheta_{T2} &= -\vartheta_{x2}\cos\theta_2 - \vartheta_{y2}\sin\theta_2 \end{aligned} \tag{2.8}$$

Substituting the equations above into the force equilibrium equations Eqs. 2.5 and 2.6 yield two simplified equations of motion:

$$\left(3-\cos 2\theta_1\right)\vartheta_{x1} + \left(\sin 2\theta_1\right)\vartheta_{y1} + \left(3-\cos 2\theta_2\right)\vartheta_{x2} - \left(\sin 2\theta_2\right)\vartheta_{y2} = 0 \tag{2.9}$$

$$\left(\sin 2\theta_1\right)\vartheta_{x1} + \left(3+\cos 2\theta_1\right)\vartheta_{y1} - \left(\sin 2\theta_2\right)\vartheta_{x2} + \left(3+\cos 2\theta_2\right)\vartheta_{y2} = -\frac{mg}{2\pi\eta_0 L} \tag{2.10}$$

For the third equation of motion, a simple moment balance is taken about point *O*. The free body diagram of Fig. 2-4 indicates that the only forces causing a moment about point *O* are the normal components of drag and the weights of the rods. The moment balance is:

$$\sum M_{z_o} = -\frac{1}{2}F_{N1}L - \frac{1}{2}F_{N2}L + \frac{1}{2}mgL\cos\theta_1 + \frac{1}{2}mgL\cos\theta_2 = 0 \tag{2.11}$$

As was done with Eqs. 2.3 and 2.4, the drag forces are expressed in terms of ϑ_{x1}, ϑ_{y1}, ϑ_{x2}, ϑ_{y2}, θ_1, and θ_2 and substituted into Eq. 2.11. The third equation of motion becomes:

$$\left(\sin\theta_1\right)\vartheta_{x1}+\left(\cos\theta_1\right)\vartheta_{y1}-\left(\sin\theta_2\right)\vartheta_{x2}+\left(\cos\theta_2\right)\vartheta_{y2}=-\frac{mg}{4\pi\eta_0 L}\left(\cos\theta_1+\cos\theta_2\right) \tag{2.12}$$

As the swimmer moves in its fluid environment and as time progress, one boundary condition must always be satisfied: the rods that constitute the arms of the swimmer are joined at point O at all times. This boundary condition affects the locomotion of the scalloping swimmer and factors into the equations of motion. The link at point O means that the velocities of the two rods at point O are equal:

$$\vec{\vartheta}_{1O}=\vec{\vartheta}_{2O} \tag{2.13}$$

where ϑ_{1O} is the velocity of the top rod at point O and ϑ_{2O} is the velocity of the bottom rod at point O. In terms of the velocities in Cartesian coordinates, with the origin at point O, the velocities are:

$$\begin{aligned}\vec{\vartheta}_{1O}&=\left(\vartheta_{x1}-\frac{1}{2}\dot{\theta}_1 L\sin\theta_1\right)\vec{e}_x+\left(\vartheta_{y1}-\frac{1}{2}\dot{\theta}_1 L\cos\theta_1\right)\vec{e}_y\\ \vec{\vartheta}_{2O}&=\left(\vartheta_{x2}-\frac{1}{2}\dot{\theta}_2 L\sin\theta_2\right)\vec{e}_x+\left(\vartheta_{y2}+\frac{1}{2}\dot{\theta}_2 L\cos\theta_2\right)\vec{e}_y\end{aligned} \tag{2.14}$$

Equating the x and y velocity components yields the two equations of motion from the velocity boundary conditions:

$$\vartheta_{x1}-\vartheta_{x2}-\frac{1}{2}\dot{\theta}_1 L\sin\theta_1+\frac{1}{2}\dot{\theta}_2 L\sin\theta_2=0 \tag{2.15}$$

$$\vartheta_{y1}-\vartheta_{y2}-\frac{1}{2}\dot{\theta}_1 L\cos\theta_1-\frac{1}{2}\dot{\theta}_2 L\cos\theta_2=0 \tag{2.16}$$

As mentioned earlier and as indicated by Fig. 2-2, the angle between the two arms of the swimmer oscillates from a small positive value θ_{min} to a larger positive value θ_{max}. The angle θ is the sum of θ_1 and θ_2 and its rate of change is prescribed to be:

$$\dot{\theta}(t) = \dot{\theta}_1 + \dot{\theta}_2 = -\frac{1}{2}\left(\theta_{max} - \theta_{min}\right)\omega \sin\omega t \tag{2.17}$$

where ω is the angular frequency of oscillation. The rate of change of θ is the forcing function and it is the sixth and last equation of motion.

Putting together the six equations, Eqs. 2.9, 2.10, 2.12, 2.15, 2.16 and 2.17, creates a system of equations relating the rates of change of the x and y coordinates of the rods, as well as the angles they make with the horizontal. Eq. 2.18 expresses the system in matrix form.

$$\begin{pmatrix} 3-\cos2\theta_1 & \sin2\theta_1 & 3-\cos2\theta_2 & -\sin2\theta_2 & 0 & 0 \\ \sin2\theta_1 & 3+\cos2\theta_1 & -\sin2\theta_2 & 3+\cos2\theta_2 & 0 & 0 \\ \sin\theta_1 & \cos\theta_1 & -\sin\theta_2 & \cos\theta_2 & 0 & 0 \\ 1 & 0 & -1 & 0 & -\sin\theta_1 & \sin\theta_2 \\ 0 & 1 & 0 & -1 & -\cos\theta_1 & -\cos\theta_2 \\ 0 & 0 & 0 & 0 & 1 & 1 \end{pmatrix} \begin{bmatrix} \vartheta_{x1} \\ \vartheta_{y1} \\ \vartheta_{x2} \\ \vartheta_{y2} \\ \dot{\theta}_1 \\ \dot{\theta}_2 \end{bmatrix} = \begin{bmatrix} 0 \\ -\dfrac{mg}{2\pi\eta_0 L} \\ -\dfrac{mg}{4\pi\eta_0 L}\left(\cos\theta_1 + \cos\theta_2\right) \\ 0 \\ 0 \\ -\dfrac{1}{2}\left(\theta_{max} - \theta_{min}\right)\omega \sin\omega t \end{bmatrix} \tag{2.18}$$

The following section discusses the numerical integration of Eq. 2.18 to obtain $x_1(t)$, $y_1(t)$, $\theta_1(t)$, $x_2(t)$, $y_2(t)$ and $\theta_2(t)$ and the Matlab simulation that allowed us to visualize the movements of the swimmer as time progressed.

2.4 Simulation and Results

Determining $x_1(t)$, $y_1(t)$, $x_2(t)$, $y_2(t)$, $\theta_1(t)$ and $\theta_2(t)$ requires numerical integration of Eq. 2.18. A Matlab code was written in order to carry out the integration with a

specified time step and to output the coordinates of the center of mass of each rod and the rod's angle with the horizontal as time progressed.

The initial conditions for the integration are $x_1(t=0)$, $y_1(t=0)$, $x_2(t=0)$, $y_2(t=0)$, $\theta_1(t=0)$ and $\theta_2(t=0)$. At $t = 0$, the scalloping swimmer is wide open and the angle between its arms is θ_{max}. Consequently, all the initial conditions are in terms of θ_{max}:

$$\begin{aligned} x_1(0) &= -\frac{L}{2}\cos\left(\frac{\theta_{max}}{2}\right) \\ y_1(0) &= \frac{L}{2}\sin\left(\frac{\theta_{max}}{2}\right) \\ \theta_1(0) &= \frac{\theta_{max}}{2} \\ x_2(0) &= -\frac{L}{2}\cos\left(\frac{\theta_{max}}{2}\right) \\ y_2(0) &= -\frac{L}{2}\sin\left(\frac{\theta_{max}}{2}\right) \\ \theta_2(0) &= \frac{\theta_{max}}{2} \end{aligned} \tag{2.19}$$

The origin of the coordinate system is placed at point *O* (see Fig. 2-4).

The simulation was carried out over two full cycles, where one full cycle is the closing and then opening of the scalloping swimmer (see Fig. 2-2). Figure 2-6 on the next page shows a graphical representation of the simulations results (only for 1.5 full cycles).

The figure shows the swimmer, in bold, and the orientation of the rods that constitute its arms at every quarter period. Each plot is superimposed on all the previous ones in gray in order to observe how far the swimmer is displaced as time progresses.

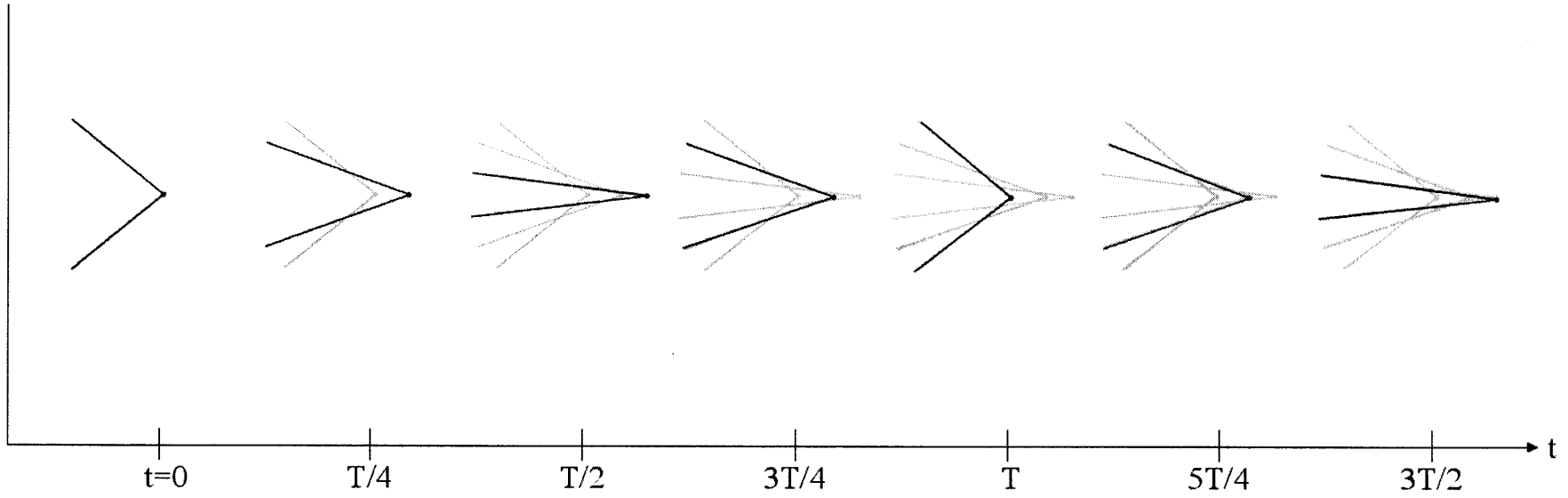

Figure 2-6: The scalloping swimmer in Newtonian fluid as time progresses. For every time interval T/4, the swimmer is depicted in bold.

2.5 Conclusions

This simulation successfully confirms that a scalloping swimmer in a Newtonian fluid experiences no net motion due to the symmetry of its movements. The results of the simulation summarized in Fig. 2-6 show that the swimmer propels itself forward at the start of each cycle, when it was closing its arms. However, as the swimmer opens its arms wide again in the second half of the cycle, it travels backward the same horizontal distance it had moved forward. Again, the swimmer experiences no net movement in the forward direction.

The simulation also served to provide us with a physical understanding of how the swimmer's locomotion works. This understanding will prove to be helpful when developing the model for the more complex case, where the swimmer is in viscoelastic fluid.

Chapter 3

Viscoelastic Model

In the previous chapter, the theoretical analysis of a two-link swimmer in a Newtonian fluid was carried out and a numerical model was developed to simulate its swimming. The numerical simulation confirmed that, in Newtonian fluid, a body comprised of two links does not have a net displacement because of the reciprocal nature of its movements. This chapter introduces a viscoelastic model, which takes into account the viscous and elastic nature of the fluid in order to determine its influence on the swimmer's propulsion. This introduction is entirely theoretical. However, future work will include a numerical simulation that is similar to, but more complex than the one carried out for the Newtonian case.

3.1 Relaxation Spectrum

As discussed in Chapter 1, a viscoelastic fluid deviates from a Newtonian fluid because accumulated stresses relax over time. The interaction between the time scale for relaxation and the period of oscillation of the swimmer's arms produces in-phase and out-of phase stresses on the swimming body [7]. The force distribution on the swimmer, and thus its swimming speed, is affected by fluid viscoelasticity.

The Maxwell model, the simplest model characterizing the stress relaxation and creep behavior of viscoelastic fluid, can be expressed in a more generalized form. The following figure shows the mechanical analogue of the generalized Maxwell model.

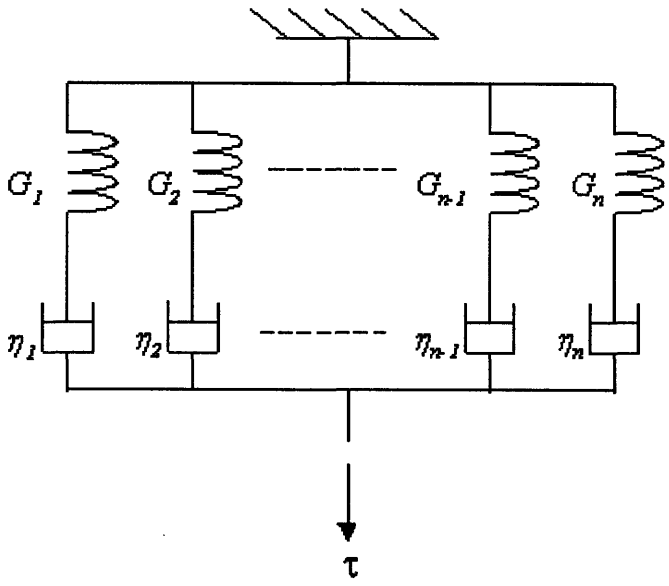

Figure 3-1: Mechanical analogue of generalized Maxwell model.

The parallel arrangement of the individual Maxwell elements, with different shear moduli, G_i, and viscosities, η_i, show that there is a distribution in the relaxation times in the generalized model. The relaxation time for each element, i, is:

$$\lambda_i = \frac{\eta_i}{G_i} \tag{3.1}$$

In general, viscoelastic fluids will exhibit a spectrum of relaxation times. Many polymeric fluids are considered viscoelastic and the spectrum of relaxation times is caused by the distribution of polymer molecular weights and amount of cross-linking [2].

In an article published in *Biorheology* in 1998, Fulford, Katz, and Powell state that the relaxation spectrum of a linear viscoelastic fluid will produce a series of different responses to a given stress or strain state [7]. Therefore, a slender rod oscillating at an angular frequency ω, much like the rods that comprise the arms of the scalloping swimmer, will elicit a response at *multiple* frequencies from the surrounding viscoelastic fluid. This is the underlying principle under which the proceeding theoretical analysis will take place.

3.2 Complex Fourier drag forces

The two slender rods that are joined and form the body of the scalloping swimmer experience translation and oscillation at a frequency ω. Thus, the velocities of the centers of mass of the rods can be decomposed into a complex Fourier series:

$$\vec{\vartheta}_1 = \sum_{m=-\infty}^{\infty} \vec{\vartheta}_1^{(m)} e^{im\omega t}$$
$$\vec{\vartheta}_2 = \sum_{m=-\infty}^{\infty} \vec{\vartheta}_2^{(m)} e^{im\omega t} \tag{3.2}$$

where ϑ_1 and ϑ_2 are the center of mass velocities of the top rod and bottom rod, respectively (refer to Fig. 2-4 to see the swimmer). The $\vartheta_1^{(m)}$ and $\vartheta_2^{(m)}$ terms refer to the Fourier coefficients (of order m) for the velocities.

Because a viscoelastic fluid has out-of-phase and in-phase behavior in response to oscillatory stresses and strains, analysis involves complex material properties. The complex viscosity is given by the following integral:

$$\eta^{(m)} = \int_0^{\infty} G_R(\tau)\, e^{-im\omega\tau}\, d\tau \tag{3.3}$$

where $\eta^{(m)}$ is the complex viscosity of order m. $G_R(t)$ is the shear relaxation modulus of the fluid. In Chapter 1, we calculated the Maxwell shear relaxation modulus to be:

$$G_R(t) = \frac{\eta_0}{\lambda} e^{-\frac{t}{\lambda}} \tag{3.4}$$

where λ is the relaxation time constant of the viscoelastic fluid. This equation is equivalent to Eq. 1.7. The m^{th} order complex viscosity then becomes:

$$\eta^{(m)} = \frac{\eta_0}{\sqrt{1 + m^2\omega^2\lambda^2}} e^{-im\omega\lambda} \tag{3.5}$$

Equations 2.1 and 2.2 still hold for the viscoelastic case because the Fourier velocity terms are linear. Therefore, the m^{th} term tangential and normal components of the drag force on a rod are independent. They are as follows:

$$F_T^{(m)} = C_T^{(m)} \vartheta_T^{(m)} L$$
$$F_N^{(m)} = C_N^{(m)} \vartheta_N^{(m)} L \tag{3.6}$$

The coefficients $C_T^{(m)}$ and $C_N^{(m)}$ are the m^{th} tangential and normal drag coefficients and they are in terms of the complex viscosity (refer to Eq. 2.2). The $\vartheta_T^{(m)}$ and $\vartheta_N^{(m)}$ terms are the Fourier coefficients of the tangential and normal components of the center of mass velocity of a rod. The rod's length is given by L. Substituting Eq. 3.5, the expression for the complex viscosity, into Eq. 3.6 and summing all the m^{th} order modes of the drag coefficient gives the total tangential and normal drag forces.

$$F_T = \sum_{m=-\infty}^{\infty} C_T^{(m)} \vartheta_T^{(m)} L e^{im\omega t} = \sum_{m=-\infty}^{\infty} \frac{2\pi\eta_0 L}{\sqrt{1+m^2\omega^2\lambda^2}} \vartheta_T^{(m)} e^{im\omega(t-\lambda)}$$
$$F_N = \sum_{m=-\infty}^{\infty} C_N^{(m)} \vartheta_N^{(m)} L e^{im\omega t} = \sum_{m=-\infty}^{\infty} \frac{4\pi\eta_0 L}{\sqrt{1+m^2\omega^2\lambda^2}} \vartheta_N^{(m)} e^{im\omega(t-\lambda)} \tag{3.7}$$

Eq. 3.7 applies to both the top rod (rod 1) and the bottom rod (rod 2). Note that the complex exponential term is offset by the relaxation time constant. The response of the fluid to the oscillation of the cylinders is out of phase, as expected.

3.3 Primary Equations of Motion

Although the free body diagram in Chapter 2 (Fig. 2-4) still applies to the viscoelastic swimmer, a small modification will be made to it based on the results obtained from the Newtonian model. Fig. 2-6, which illustrates the results of the Newtonian simulation, shows that the net horizontal displacement of the swimmer over one cycle is zero. What the figure does not show well is that the swimmer is sinking over time. This is because the vertical displacement, due to the influence of gravity, is small

compared to the displacements in the horizontal direction and small compared to the size of the swimmer. Thus, gravity will not be factored into equations of motion for the swimmer in viscoelastic fluid (refer to the free body diagram in Fig. 3-2).

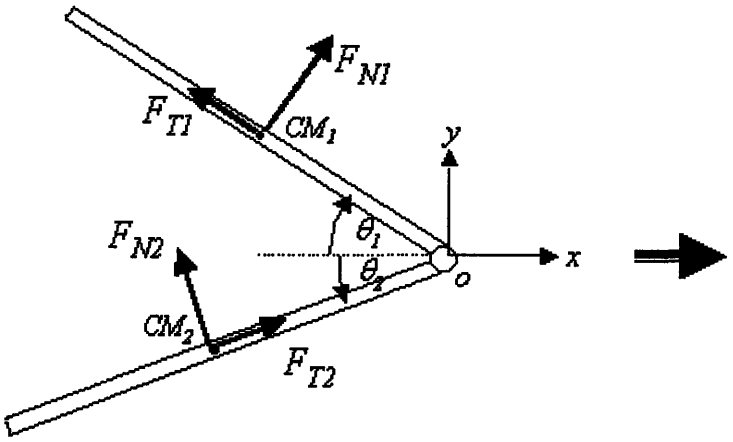

Figure 3-2: Free body diagram of swimmer in viscoelastic fluid. The weights of the rods are neglected.

As noted for the Newtonian model, there are six independent equations relating the drag forces on and the angles of the rotating rods. With the modifications discussed above, they are now:

$$\sum F_x = F_{N1}\sin\theta_1 - F_{T1}\cos\theta_1 - F_{N2}\sin\theta_2 + F_{T2}\cos\theta_2 = 0 \tag{3.8}$$

$$\sum F_y = F_{N1}\cos\theta_1 + F_{T1}\sin\theta_1 + F_{N2}\cos\theta_2 + F_{T2}\sin\theta_2 = 0 \tag{3.9}$$

$$\sum M_{z_o} = -\frac{1}{2}F_{N1}L - \frac{1}{2}F_{N2}L = 0 \tag{3.10}$$

$$\vartheta_{x1} - \vartheta_{x2} - \frac{1}{2}\dot{\theta}_1 L\sin\theta_1 + \frac{1}{2}\dot{\theta}_2 L\sin\theta_2 = 0 \tag{3.11}$$

$$\vartheta_{y1} - \vartheta_{y2} - \frac{1}{2}\dot{\theta}_1 L\cos\theta_1 - \frac{1}{2}\dot{\theta}_2 L\cos\theta_2 = 0 \tag{3.12}$$

$$\dot{\theta}_1 + \dot{\theta}_2 = \dot{\theta}(t) \tag{3.13}$$

These primary equations of motion, as stated, solve only six unknowns. For the Newtonian model, there were six unknowns: $\vartheta_{x1}(t)$, $\vartheta_{y1}(t)$, $\dot{\theta}_1(t)$, $\vartheta_{x2}(t)$, $\vartheta_{y2}(t)$ and $\dot{\theta}_2(t)$. Numerical integration yielded $x_1(t)$, $y_1(t)$, $\theta_1(t)$, $x_2(t)$, $y_2(t)$ and $\theta_2(t)$.

For the viscoelastic case, the x and y velocities of the centers of mass of the rods are expressed in terms of complex Fourier series. The unknowns for each component of the velocities are the number of Fourier coefficients. In order to best understand how this works, let us assume that Eq. 3.2 is not an infinite sum, that there are a finite number of complex Fourier coefficients for each velocity:

$$\begin{aligned} \vartheta_{x1} &= \sum_{m=-n}^{n} \vartheta_{x1}^{(m)} e^{im\omega t} \\ \vartheta_{y1} &= \sum_{m=-n}^{n} \vartheta_{y1}^{(m)} e^{im\omega t} \end{aligned} \tag{3.14}$$

$$\begin{aligned} \vartheta_{x2} &= \sum_{m=-n}^{n} \vartheta_{x2}^{(m)} e^{im\omega t} \\ \vartheta_{y2} &= \sum_{m=-n}^{n} \vartheta_{y2}^{(m)} e^{im\omega t} \end{aligned} \tag{3.15}$$

Eq. 3.14 is the complex Fourier series for the center of mass velocity of the top rod and Eq. 3.15 is the complex Fourier series for the center of mass velocity of the bottom rod. $\vartheta_{x1}(t)$, $\vartheta_{y1}(t)$, $\vartheta_{x2}(t)$, and $\vartheta_{y2}(t)$ are real valued functions of time, even though they are complex sums (the imaginary parts cancel out).

Each velocity component, in this case, has $2n + 1$ Fourier coefficients and there are a total of $8n + 4$ unknown m^{th} term velocities. Along with the θ_1 and θ_2, that makes a total of $8n + 6$ unknowns that need to be solved for. Hence, $8n + 6$ independent equations are required. The following section discusses how to obtain more independent equations that are imbedded within the set of six that were used in the Newtonian case (Eqs. 3.8-3.13).

3.4 Secondary Equations of Motion

3.4.1 Finite Limits for Complex Sums

One equation of motion that will retain the same form in the viscoelastic case is the forcing function on the angle between the arms of the scalloping swimmer. Eq. 3.13 gives a generic form of the equation of motion because $\dot{\theta}(t)$ can theoretically be any periodic function of frequency ω. For convenience, $\dot{\theta}(t)$ will remain the same:

$$\dot{\theta}_1 + \dot{\theta}_2 = -\frac{1}{2}\left(\theta_{max} - \theta_{min}\right)\omega \sin\omega t \tag{3.16}$$

The results from the Newtonian swimmer simulation showed that, because the moment on each rod was equal and opposite, $\theta_1(t)$ and $\theta_2(t)$ were the same for all time. Therefore, it can be said that:

$$\theta_1 = \theta_2 = \theta' \tag{3.17}$$

Using θ' will be useful in the following calculations.

Looking at the equations of motion for the Newtonian swimmer, Eq. 2.18, there seem to be a few expressions of $\sin\theta'$, $\cos\theta'$, $\sin 2\theta'$, and $\cos 2\theta'$. Because θ' is not a constant value but a periodic function, all the trigonometric functions of θ' will be periodic and have frequencies related to ω. Here are the relevant trig functions and their complex Fourier series:

$$3 - \cos 2\theta' = \sum_{l=-\infty}^{\infty} \alpha_l \, e^{il\,2\omega(t-\lambda)} \tag{3.18}$$

$$\sin 2\theta' = \sum_{l=-\infty}^{\infty} \beta_l \, e^{il\,2\omega(t-\lambda)} \tag{3.19}$$

$$3 + \cos 2\theta' = \sum_{l=-\infty}^{\infty} \gamma_l \, e^{il\,2\omega(t-\lambda)} \tag{3.20}$$

$$\cos\theta' = \sum_{l=-\infty}^{\infty} A_l \, e^{il\,\omega t} \tag{3.21}$$

$$\sin\theta' = \sum_{l=-\infty}^{\infty} B_l e^{il\omega t} \tag{3.22}$$

The terms α_l, β_l, γ_l, A_l and B_l are the complex Fourier coefficients of their respective trigonometric functions. The Fourier series related in Eqs. 3.18-3.20 are centered about $t = \lambda$ for convenience, as will be seen later.

Determining the complex Fourier coefficients of known functions can be difficult depending on what the function is. For Eqs. 3.18-3.22, the functions are trigonometric functions of a trigonometric function, θ'. This makes determining the Fourier coefficients challenging, at least analytically. Therefore, α_l, β_l, γ_l, A_l and B_l will be determined numerically. This can be done by converting each trigonometric function into a discrete data set and inputting it into Matlab's fast fourier transform algorithm, FFT. FFT outputs the complex Fourier coefficients of the function. As this is a numerical calculation, the more discrete data points that are provided, the larger the number of coefficients that can be found and the more accurate they are.

It is expected that there will be a finite number of relevant Fourier coefficients for the trigonometric functions above; that is, there will be more frequency modes close to ω and the modes farther away are insignificant. Thus, Eqs. 3.18-3.22 can be written as finite sums:

$$3 - \cos 2\theta' = \sum_{l=-k}^{k} \alpha_l e^{il2\omega(t-\lambda)} \tag{3.23}$$

$$\sin 2\theta' = \sum_{l=-k}^{k} \beta_l e^{il2\omega(t-\lambda)} \tag{3.24}$$

$$3 + \cos 2\theta' = \sum_{l=-k}^{k} \gamma_l e^{il2\omega(t-\lambda)} \tag{3.25}$$

$$\cos\theta' = \sum_{l=-k}^{k} A_l e^{il\omega t} \tag{3.26}$$

$$\sin\theta' = \sum_{l=-k}^{k} B_l e^{il\omega t} \tag{3.27}$$

The limit index k can be determined manually by looking at the Fourier coefficients that the FFT algorithm outputs.

Because the limits on the complex Fourier series for the trigonometric functions above are finite, we will see that that makes the number of unknown velocity coefficients finite as well.

3.4.2 Velocity boundary conditions

In order to most clearly demonstrate how the equations of motion are going to be obtained from Eqs. 3.8-3.13 and Eqs. 3.23-3.27, let us assume that the limit index k is 1. With substitutions from Eq. 3.14, 3.15, 3.26, and 3.27, the equations for the velocity boundary conditions, Eqs. 3.11 and 3.12, become:

$$\sum_{m=-\infty}^{\infty} \vartheta_{x1}^{(m)} e^{im\omega t} - \sum_{m=-\infty}^{\infty} \vartheta_{x2}^{(m)} e^{im\omega t} - \frac{1}{2}\dot{\theta}_1 L \sum_{l=-1}^{1} B_l e^{il\omega t} + \frac{1}{2}\dot{\theta}_2 L \sum_{l=-1}^{1} B_l e^{il\omega t} = 0 \tag{3.28}$$

$$\sum_{m=-\infty}^{\infty} \vartheta_{y1}^{(m)} e^{im\omega t} - \sum_{m=-\infty}^{\infty} \vartheta_{y2}^{(m)} e^{im\omega t} - \frac{1}{2}\dot{\theta}_1 L \sum_{l=-1}^{1} A_l e^{il\omega t} - \frac{1}{2}\dot{\theta}_2 L \sum_{l=-1}^{1} A_l e^{il\omega t} = 0 \tag{3.29}$$

Eqs. 3.28 and 3.29 have to hold for all time. Therefore, the coefficients of each mode must sum to zero. This summing produces the extra equations needed to solve for the unknown terms. The equations obtained from above are:

$$\begin{aligned}
&\vartheta_{x1}^{(1)} - \vartheta_{x2}^{(1)} - \frac{1}{2}\dot{\theta}_1 L B_1 + \frac{1}{2}\dot{\theta}_2 L B_1 = 0 \\
&\vartheta_{x1}^{(0)} - \vartheta_{x2}^{(0)} - \frac{1}{2}\dot{\theta}_1 L B_0 + \frac{1}{2}\dot{\theta}_2 L B_0 = 0 \\
&\vartheta_{x1}^{(-1)} - \vartheta_{x2}^{(-1)} - \frac{1}{2}\dot{\theta}_1 L B_{-1} + \frac{1}{2}\dot{\theta}_2 L B_{-1} = 0
\end{aligned} \tag{3.30}$$

$$\vartheta_{y1}^{(1)} - \vartheta_{y2}^{(1)} - \frac{1}{2}\dot{\theta}_1 L A_1 - \frac{1}{2}\dot{\theta}_2 L A_1 = 0$$
$$\vartheta_{y1}^{(0)} - \vartheta_{y2}^{(0)} - \frac{1}{2}\dot{\theta}_1 L A_0 - \frac{1}{2}\dot{\theta}_2 L A_0 = 0 \qquad (3.31)$$
$$\vartheta_{y1}^{(-1)} - \vartheta_{y2}^{(-1)} - \frac{1}{2}\dot{\theta}_1 L A_{-1} - \frac{1}{2}\dot{\theta}_2 L A_{-1} = 0$$

Notice that m is restricted to the interval $-k < m < k$. Equations for m beyond the interval are redundant; that is they yield trivial solutions for the velocity terms. The coefficients A_l and B_l are known. They are to be determined by the FFT algorithm.

Because m is now in the interval $-k < m < k$, there are $8k + 6 = 14$ unknowns that are going to be solved for. At this point, seven equations of motion (Eqs. 3.16, 3.30, and 3.31) are known and seven more need to be determined.

3.4.3 Force and Moment Equilibrium

To begin, the first primary equilibrium equation, Eq. 3.8, can be dissected. Substituting the complex drag force terms of Eq. 3.7, performing a vector transformation to obtain the x and y components of the velocities, and substituting in Eqs. 3.14 and 3.15 yields the following:

$$\left[\sum_{m=-\infty}^{\infty} \frac{e^{im\omega(t-\lambda)}}{\sqrt{1+m^2\omega^2\lambda^2}} \vartheta_{x1}^{(m)}\right](3-\cos 2\theta') + \left[\sum_{m=-\infty}^{\infty} \frac{e^{im\omega(t-\lambda)}}{\sqrt{1+m^2\omega^2\lambda^2}} \vartheta_{y1}^{(m)}\right](\sin 2\theta')$$
$$+\left[\sum_{m=-\infty}^{\infty} \frac{e^{im\omega(t-\lambda)}}{\sqrt{1+m^2\omega^2\lambda^2}} \vartheta_{x2}^{(m)}\right](3-\cos 2\theta') - \left[\sum_{m=-\infty}^{\infty} \frac{e^{im\omega(t-\lambda)}}{\sqrt{1+m^2\omega^2\lambda^2}} \vartheta_{T2}^{(m)}\right](\sin 2\theta') = 0 \qquad (3.32)$$

The trigonometric terms are Fourier series as well (Eqs. 3.23-3.27) and the sums can be combined to yield a double sum over m and l:

$$\sum_{m=-1}^{1}\sum_{l=-1}^{1}\frac{e^{i\omega(2l+m)(t-\lambda)}}{\sqrt{1+m^2\omega^2\lambda^2}}\alpha_l\vartheta_{x1}^{(m)}+\frac{e^{i\omega(2l+m)(t-\lambda)}}{\sqrt{1+m^2\omega^2\lambda^2}}\beta_l\vartheta_{y1}^{(m)}+\frac{e^{i\omega(2l+m)(t-\lambda)}}{\sqrt{1+m^2\omega^2\lambda^2}}\alpha_l\vartheta_{x2}^{(m)}-\frac{e^{i\omega(2l+m)(t-\lambda)}}{\sqrt{1+m^2\omega^2\lambda^2}}\beta_l\vartheta_{y2}^{(m)}=0 \tag{3.33}$$

Carrying out the sum over l and m is manageable because $k = 1$, but for larger k the sum will be difficult to perform by hand. Summing and matching the coefficients for the exponential terms, ultimately yields the following three independent equations:

$$\begin{aligned}
&\alpha_0\vartheta_{x1}^{(1)}+\beta_0\vartheta_{y1}^{(1)}+\alpha_0\vartheta_{x2}^{(1)}-\beta_0\vartheta_{y2}^{(1)}+\alpha_1\vartheta_{x1}^{(-1)}+\beta_1\vartheta_{y1}^{(-1)}+\alpha_1\vartheta_{x2}^{(-1)}-\beta_1\vartheta_{y2}^{(-1)}=0\\
&\alpha_0\vartheta_{x1}^{(0)}+\beta_0\vartheta_{y1}^{(0)}+\alpha_0\vartheta_{x2}^{(0)}-\beta_0\vartheta_{y2}^{(0)}=0\\
&\alpha_{-1}\vartheta_{x1}^{(1)}+\beta_{-1}\vartheta_{y1}^{(1)}+\alpha_{-1}\vartheta_{x2}^{(1)}-\beta_{-1}\vartheta_{y2}^{(1)}+\alpha_0\vartheta_{x1}^{(-1)}+\beta_0\vartheta_{y1}^{(-1)}+\alpha_0\vartheta_{x2}^{(-1)}-\beta_0\vartheta_{y2}^{(-1)}=0
\end{aligned} \tag{3.34}$$

The Fourier coefficients α_l and β_l are known, so the only unknowns in Eq. 3.34 are the $m = -1$ and $m = 1$ Fourier coefficients of each velocity component.

The double sum in Eq. 3.33 actually yields nine equations instead of three, but many of these equations were eliminated because they were not independent of each other. Take for example the following two equations that were obtained from the sum in Eq. 3.33:

$$\begin{aligned}
&\alpha_1\vartheta_{x1}^{(1)}+\beta_1\vartheta_{y1}^{(1)}+\alpha_1\vartheta_{x2}^{(1)}-\beta_1\vartheta_{y2}^{(1)}=0\\
&\alpha_{-1}\vartheta_{x1}^{(-1)}+\beta_{-1}\vartheta_{y1}^{(-1)}+\alpha_{-1}\vartheta_{x2}^{(-1)}-\beta_{-1}\vartheta_{y2}^{(-1)}=0
\end{aligned} \tag{3.35}$$

The two equations above are nearly identical except that the index for the Fourier coefficients for the trigonometric terms and the Fourier coefficients for the velocity terms are opposite signs. When a real valued function is expressed in a complex Fourier series, the sum of all the complex terms must be real. Therefore, each Fourier coefficient is the complex conjugate of the coefficient that has the negative of its index. For example, α_l

and α_{-1} are complex conjugates, as are $\vartheta_{x1}^{(1)}$ and $\vartheta_{x1}^{(-1)}$, the $m = 1$ and $m = -1$ modes of the top rod's x component velocity. Consequently, the two equations in Eq. 3.35 are complex conjugates of each other, making them non-independent equations. The other equations were eliminated in the same manner.

The force balance in the y direction, after much manipulation yields the following set of equations:

$$\beta_0\vartheta_{x1}^{(1)}+\gamma_0\vartheta_{y1}^{(1)}-\beta_0\vartheta_{x2}^{(1)}+\gamma_0\vartheta_{y2}^{(1)}+\beta_1\vartheta_{x1}^{(-1)}+\gamma_1\vartheta_{y1}^{(-1)}-\beta_1\vartheta_{x2}^{(-1)}+\gamma_1\vartheta_{y2}^{(-1)}=0$$

$$\beta_0\vartheta_{x1}^{(0)}+\gamma_0\vartheta_{y1}^{(0)}-\beta_0\vartheta_{x2}^{(0)}+\gamma_0\vartheta_{y2}^{(0)}=0$$

$$\beta_{-1}\vartheta_{x1}^{(1)}+\gamma_{-1}\vartheta_{y1}^{(1)}-\beta_{-1}\vartheta_{x2}^{(1)}+\gamma_{-1}\vartheta_{y2}^{(1)}+\beta_0\vartheta_{x1}^{(-1)}+\gamma_0\vartheta_{y1}^{(-1)}-\beta_0\vartheta_{x2}^{(-1)}+\gamma_0\vartheta_{y2}^{(-1)}=0 \tag{3.36}$$

And the moment equilibrium yields only one independent equation:

$$\frac{B_{-1}}{\sqrt{1+\omega^2\lambda^2}}\vartheta_{x1}^{(1)}+\frac{A_{-1}}{\sqrt{1+\omega^2\lambda^2}}\vartheta_{y1}^{(1)}-\frac{B_{-1}}{\sqrt{1+\omega^2\lambda^2}}\vartheta_{x2}^{(1)}+\frac{A_{-1}}{\sqrt{1+\omega^2\lambda^2}}\vartheta_{y2}^{(1)}$$
$$+B_0\vartheta_{x1}^{(0)}+A_0\vartheta_{y1}^{(0)}-B_0\vartheta_{x2}^{(0)}+A_0\vartheta_{y2}^{(0)}$$
$$+\frac{B_1}{\sqrt{1+\omega^2\lambda^2}}\vartheta_{x1}^{(-1)}+\frac{A_1}{\sqrt{1+\omega^2\lambda^2}}\vartheta_{y1}^{(-1)}-\frac{B_1}{\sqrt{1+\omega^2\lambda^2}}\vartheta_{x2}^{(-1)}+\frac{A_1}{\sqrt{1+\omega^2\lambda^2}}\vartheta_{y2}^{(-1)}=0 \tag{3.37}$$

The 14 equations given by Eqs. 3.16, 3.30, 3.31, 3.34, 3.36, and 3.37 can be solved numerically to solve for the Fourier velocity terms of m^{th} order and, in turn, the center of mass position of each rod as time progress. The positions, as well as the angles of the rod, will provide the necessary inputs for a numerical simulation of the swimmer scalloping in viscoelastic fluid. A numerical simulation has not been performed to validate the theoretical model developed; however, the next section discusses the steps necessary to simulate the two-link swimmer in viscoelastic fluid.

3.5 Setup for Simulation

As was the case with the swimmer scalloping in a Newtonian fluid, the time-varying quantities that we want to solve for are $x_1(t)$, $y_1(t)$, $\theta_1(t)$, $x_2(t)$, $y_2(t)$ and $\theta_2(t)$. These quantities, when shown graphically in a simulation, show how the swimmer moves in a fluid.

The time-varying positions are found by numerically integrating the equations of motion. For a Fourier index limit $k = 1$, the equations of motion can be expression as a linear system:

$$[A]\cdot\begin{bmatrix} \vartheta_{x1}^{(1)} \\ \vartheta_{y1}^{(1)} \\ \vartheta_{x2}^{(1)} \\ \vartheta_{y2}^{(1)} \\ \vartheta_{x1}^{(0)} \\ \vartheta_{y1}^{(0)} \\ \vartheta_{x2}^{(0)} \\ \vartheta_{y2}^{(0)} \\ \vartheta_{x1}^{(-1)} \\ \vartheta_{y1}^{(-1)} \\ \vartheta_{x2}^{(-1)} \\ \vartheta_{y2}^{(-1)} \\ \dot{\theta}_1 \\ \dot{\theta}_2 \end{bmatrix} = \begin{bmatrix} 0 \\ 0 \\ 0 \\ 0 \\ 0 \\ 0 \\ 0 \\ 0 \\ 0 \\ 0 \\ 0 \\ 0 \\ 0 \\ -\frac{1}{2}\left(\theta_{max}-\theta_{min}\right)\omega\sin\omega t \end{bmatrix} \tag{3.38}$$

where A is a matrix of coefficients that is invertible at each time step of integration. It is given by Eq. 3.39 on the next page.

$$
[A]=\begin{bmatrix}
\alpha_0 & \beta_0 & \alpha_0 & -\beta_0 & 0 & 0 & 0 & 0 & \alpha_1 & \beta_1 & \alpha_1 & -\beta_1 & 0 & 0 \\
0 & 0 & 0 & 0 & \alpha_0 & \beta_0 & \alpha_0 & -\beta_0 & 0 & 0 & 0 & 0 & 0 & 0 \\
\alpha_{-1} & \beta_{-1} & \alpha_{-1} & -\beta_{-1} & 0 & 0 & 0 & 0 & \alpha_0 & \beta_0 & \alpha_0 & -\beta_0 & 0 & 0 \\
\beta_0 & \gamma_0 & -\beta_0 & \gamma_0 & 0 & 0 & 0 & 0 & \beta_1 & \gamma_1 & -\beta_1 & \gamma_1 & 0 & 0 \\
0 & 0 & 0 & 0 & \beta_0 & \gamma_0 & -\beta_0 & \gamma_0 & 0 & 0 & 0 & 0 & 0 & 0 \\
\beta_{-1} & \gamma_{-1} & -\beta_{-1} & \gamma_{-1} & 0 & 0 & 0 & 0 & \beta_0 & \gamma_0 & -\beta_0 & \gamma_0 & 0 & 0 \\
\dfrac{B_{-1}}{\sqrt{1+\omega^2\lambda^2}} & \dfrac{A_{-1}}{\sqrt{1+\omega^2\lambda^2}} & \dfrac{B_{-1}}{\sqrt{1+\omega^2\lambda^2}} & \dfrac{A_{-1}}{\sqrt{1+\omega^2\lambda^2}} & B_0 & A_0 & -B_0 & A_0 & \dfrac{B_1}{\sqrt{1+\omega^2\lambda^2}} & \dfrac{A_1}{\sqrt{1+\omega^2\lambda^2}} & \dfrac{B_1}{\sqrt{1+\omega^2\lambda^2}} & \dfrac{A_1}{\sqrt{1+\omega^2\lambda^2}} & 0 & 0 \\
1 & 0 & -1 & 0 & 0 & 0 & 0 & 0 & 0 & 0 & 0 & 0 & -\frac{1}{2}LB_1 & \frac{1}{2}LB_1 \\
0 & 0 & 0 & 0 & 1 & 0 & -1 & 0 & 0 & 0 & 0 & 0 & -\frac{1}{2}LB_0 & \frac{1}{2}LB_0 \\
0 & 0 & 0 & 0 & 0 & 0 & 0 & 0 & 1 & 0 & -1 & 0 & -\frac{1}{2}LB_{-1} & \frac{1}{2}LB_{-1} \\
0 & 1 & 0 & -1 & 0 & 0 & 0 & 0 & 0 & 0 & 0 & 0 & -\frac{1}{2}LA_1 & -\frac{1}{2}LA_1 \\
0 & 0 & 0 & 0 & 0 & 1 & 0 & -1 & 0 & 0 & 0 & 0 & -\frac{1}{2}LA_0 & -\frac{1}{2}LA_0 \\
0 & 0 & 0 & 0 & 0 & 0 & 0 & 0 & 0 & 1 & 0 & -1 & -\frac{1}{2}LA_{-1} & -\frac{1}{2}LA_{-1} \\
0 & 0 & 0 & 0 & 0 & 0 & 0 & 0 & 0 & 0 & 0 & 0 & 1 & 1
\end{bmatrix}
$$

Eq. (3.39)

The matrix A is multiplying a vector of the unknown quantities that are being calculated for each time step of integration. All the modes of each velocity component are summed to find the total velocity of each rod.

$$\begin{aligned} \vartheta_{x1} &= \sum_{m=-1}^{1} \vartheta_{x1}^{(m)} e^{im\omega t} \\ \vartheta_{y1} &= \sum_{m=-1}^{1} \vartheta_{y1}^{(m)} e^{im\omega t} \end{aligned} \tag{3.40}$$

$$\begin{aligned} \vartheta_{x2} &= \sum_{m=-1}^{1} \vartheta_{x2}^{(m)} e^{im\omega t} \\ \vartheta_{y2} &= \sum_{m=-1}^{1} \vartheta_{y2}^{(m)} e^{im\omega t} \end{aligned} \tag{3.41}$$

Integration leads to the positions of the rods' centers of mass at each interval of time. The initial conditions remain the same and they are given by Eq. 2.19.

The simulation ought to run for a few whole cycles so that any horizontal displacement of the swimmer can be readily discernible and the displacement per cycle can be determined.

Chapter 4

Discussion and Future Work

As E.M. Purcell established in his famous lecture on *Life at low Reynolds number*, a rigid swimmer composed of two links will experience no net displacement if it attempts to swim in a Newtonian fluid. This is due to the reciprocal nature of the swimmer's movements. The Newtonian two-link swimmer was modeled and its movement was simulated in order to confirm that E.M. Purcell's Scallop Theorem was indeed correct.

Future work entails integrating the theoretical complex Fourier analysis into a numerical scheme that will allow us to see whether the rigid swimmer can actually move about in viscoelastic fluid, despite the swimmer's reciprocal motions. This will validate the theoretical model that has been developed in this paper.

In order to be able to efficiently perform the numerical simulation two techniques need to be refined and automated:

(1) It is assumed that the complex Fourier series for the trigonometric functions of $\theta'(t)$ converge to finite sums. At this point, determining the limit index k must be done manually. Matlab, or any other programming tool, should be used to automatically obtain the value of k for which the series converge.

(2) For the case where the limit index was $k = 1$, the sums for the primary equations of motion were written out by hand. As stated earlier in the paper, many of the secondary equations of motion were found to be redundant and were discarded. The process was done manually as well. For values of k larger than 1, this will be an arduous task.

Aside from these two challenges that will need to be overcome in order to efficiently simulate the scalloping of the rigid swimmer in viscoelastic fluid, the theoretical analysis performed looks promising. The complex Fourier analysis takes into account the behavior of the viscoelastic fluid that deviates from the Newtonian fluid.

Furthermore, modeling of locomotion and swimming in viscoelastic fluid is more applicable to real world creatures like flagellar bacteria and mucous covered snails.

References

[1] Purcell, E.M. "Life at low Reynolds number." *American Journal of Physics*. 45.1 (1977): 3-11.

[2] Darby, Ronald. *Viscoelastic Fluids*. New York: Marcel Dekker, Inc, 1976.

[3] Gerhart, Philip M., Gross, Richard J., and John I. Hochstein. *Fundamentals of Fluid Mechanics*. Reading, MA: Addison-Wesley, 1992.

[4] Knight, Will. "Drugs delivered by robots in the blood." *New Scientist*. (1 Oct. 2004). 16 April 2007. <http://www.newscientist.com/article.ns?id=dn6474>.

[5] Graham-Rowe, Duncan. "Batteryless implant measures blood pressure in heart." *New Scientist*. (28 Feb. 2004). 16 April 2007. <http://www.newscientist.com/article.ns?id=dn4715>.

[6] Penman, Dan. "Tiny corkscrew pulls blood clots from brain." *New Scientist*. (5 Feb. 2004). 16 April 2007. < http://www.newscientist.com/article.ns?id=dn4647>.

[7] Fulford, G.R., Katz D.F., and R. L. Powell. "Swimming of spermatozoa in a linear viscoelastic fluid." *Biorheology*. 35.4 (1998). 295-309.